Supplementary Information

A novel green synthesis of zinc sulfide nanoparticles using *Artemisia Herba Alba* plant extract for adsorption and photocatalysis of methyl blue dye

2. Experimental details

Chemicals and reagents together with Artemisia Herba Alba plant extraction were demonstrated in the first section of the Supplementary Materials.

2.1. Chemicals and Reagents

Analytical-grade chemicals were used from commercial sources without any further purification. Zinc (II) acetate dihydrate (Zn $[CH_3COO]_2.2H_2O \geq 98\%$), sodium sulfide ($Na_2S \geq 98\%$), and methylene blue dye ($C_{16}H_{18}ClN_3S \geq 50\%$, MW = 319,85 g/mol) were purchased from Sigma-Aldrich. Ultra-pure water (UPW) from the Millipore system was employed in all aqueous solutions (resistivity > 18 MOhm.com).

2.2. *Artemisia Herba Alba* extraction

Artemisia Herba Alba (AHA) plants were collected from Tunisia. The selected leaves of AHA plants were washed with deionized water and then dried in the shade at room temperature and ground into powder. 11.5 g of powder was added to 200 mL of distilled water. The mixtures were boiled at 100 °C for 2h and filtered at room temperature. The filtered aqueous solution constitutes the extract of *A. herba alba*, which was used for ZnS nanoparticle fabrication in the present study. **Fig. S1** shows a picture of *A. herba alba* leaves and their extract.

Fig.S1: *Artemisia Herba Alba* plant and its extract.

2.3. Synthesis of ZnS nanoparticles

The colloidal wet chemical route has been used to describe in detail how ZnS nanoparticles are made [1]. The green synthesis of the ZnS NPs was carried out employing *Artemisia Herba Alba* (AHA) extract as a complexing agent. In the typical synthesis process of AHA-capped

ZnS NPs, 20 ml of AHA aqueous extract was mixed with 3 mM of $Zn[OOCCH_3]_2 \cdot 2H_2O$ solution (50 ml). The mixture was then agitated and degassed in the presence of N_2 for 30 min. In a second step, under stirring, 1.2 mM of Na_2S solution (30 ml) was added to the solution containing Zn-AHA complexes at room temperature. Then, the mixture was heated under N_2 reflux at 100 °C for 3 h to obtain AHA-capped ZnS NPs. The final solution was to allow the solution to cool down naturally at room temperature to stop the growth of NPs. The nanoparticle powder was separated by centrifugation for 20 min and washed with water and ethanol, and then it was stored at room temperature to be used later in dye removal studies.

2.4. Adsorbent characterization

Numerous techniques were used to characterize AHA-capped ZnS NPs. XRD measurements were carried out using a Panalytical X' Pert Pro diffractometer with a CuKα radiation source (λ=1,542Å). Fourier transform infrared (FTIR) spectra were obtained in the transmission mode using a Perkin Elmer version 5.3 spectrophotometer in the spectral range of 400–4000 cm^{-1} at room temperature using KBr pellet disks. High-resolution transmission electron microscopy (HR-TEM) images were recorded using a JEM-2100 microscope operating at 200 kV and equipped with an Energy Dispersive X-ray (EDX) system for element chemical analysis. A drop of nanocrystal solution was poured onto carbon-coated copper grids to obtain HR-TEM samples, where the excess solvent was evaporated. The nanocrystal size and size-distribution data were collected based on the HR-TEM images by measuring at least 100 randomly selected nanocrystals using an image processing program (ImageJ, version 1.50). Absorbance spectra were registered using a SPECORD 210 Plus spectrophotometer in the range of 200–800 nm at room temperature with a quartz cuvette. Photoluminescence (PL) spectroscopy was used to study the defects and emission properties of the ZnS NAs using a helium-cadmium laser as an exciting source of 325 nm.

2.5. Dye adsorption experiments

The process of molecules or particles sticking to the surface of a material or substrate is called adsorption. The study of the adsorption of MB onto AHA capped ZnS nanoparticles involves investigating the interaction between the dye and the surface of the nanoparticles. This can be done by preparing a suspension of the nanoparticles and adding a known concentration of MB to it. After stirring and allowing the suspension to equilibrate for a period of time, the concentration of MB remaining in the solution is measured using a UV-Vis

spectrophotometer (SPECORD 210 Plus, Tunisia). All adsorption tests were performed with magnetic stirring in the dark.

You can figure out how well the nanoparticles absorb by figuring out the difference between how much MB was in the solution at the beginning and how much was left at the end. This information can be used to figure out how well the nanoparticles remove MB from the water. Factors that can affect the adsorption of MB on AHA capped ZnS nanoparticles include the concentration of MB, the pH of the solution, the temperature, and the size and surface area of the nanoparticles. These parameters can be varied to optimize the adsorption capacity of the nanoparticles. To check the effect of these parameters, each one was tested individually by holding all the other variables fixed. Contact time (0-120 min), initial concentrations of MB (10-30 mg/l), adsorbent dose (0.1-2 g/l), different medium pH (5-9) and temperature range (298-318 K) were studied to find the effect of these variables on the adsorption operation of ZnS nanoparticles in aqueous solutions. The MB adsorbed amount Qe (mg/g) as well as the percent dye removal efficiency (%) by the ZnS NPs can be expressed as [2]:

$$Q_e = \frac{(C_0 - C_e)V}{m} \quad (1)$$

$$Dye\ Adsorption\ efficiency\ (\%) = \frac{(C_0 - C_e)}{C_0} x\ 100 \quad (2)$$

where C_0 and C_e is the initial and the equilibrium concentrations of dye in the solution, in (mg/L), respectively, V is the volume of the MB solution in (mL), and m is the mass of the ZnS-AHA in (mg). The plot of equilibrium adsorption capacity Q_e against equilibrium concentration C_e in the liquid phase is graphically illustrated to determine the equilibrium isotherm.

Furthermore, the density ρ was calculated using the following expression [2]:

$$\rho = \frac{ZM}{N_A V} \quad (3)$$

Where Z is the number of atoms per unit cell, M (g mol^{-1}) is the molecular weight of the ZnS, V is the volume of the unit cell (cm^{-3}) and N_A is the Avogadro number. The specific surface area S (cm^2 g^{-1}) of ZnS nano-particles was calculated using the next equation [2]:

$$S = \frac{6}{\rho D} \quad (4)$$

Where ρ (g cm^{-1}) and D (nm) are the x-ray density of cubic or hexagonal nano-particles and the average particle size, respectively.

2.6. Photocatalytic degradation measurements

The photocatalytic performance of ZnS-AHA NPs was measured by the photodegradation of MB as model dye. The photocatalytic experiments were carried out at 300 K and pH 7 with the initial concentration and volume of 10 mg/l and 20 ml respectively in the presence of 20 mg ZnS NAs. At midday on a clear day in Tunisia, the intensity of sunlight at the Earth's surface is typically around 1000 watts per square meter (W/m²). By contrast to sunlight, UV radiation represented only 5% (50 Wm^{-2}) of the total available solar flux received at the surface of the earth in the most favorable sunlight conditions [1]. After the adsorption phase (in the dark), the suspensions were submitted to sunlight irradiation between 11 am and 2 pm to rate the dye degradation. The photocatalytic activity was examined by monitoring the concentration in samples of 2 mL of the preparation suspension taken after filtration at different irradiation periods (0, 10, 20, 30, 45, 60, 120, 180 min). According to the Beer-Lambert law, the degradation performance was evaluated by measuring the optical absorption at the maximum absorption wavelength of MB at 664 [2]. The degradation efficiency and rate were calculated using the following equations [2]:

$$\eta = \frac{C_0 - C_t}{C_0} \text{ x } 100 \quad (5)$$

$$kt = Ln\left(\frac{C_0}{C_t}\right) \quad (6)$$

$$t_{1/2} = \frac{Ln(2)}{K} \quad (7)$$

Where $C_0, C,$ are the concentrations (mg/L) and A_0 and A are the absorbances of MB dye solution before and after irradiation, respectively, at different times using the NPs. Note that K (min^{-1}) is the apparent reaction rate constant, which is calculated from of *Ln* (C/C_0) or *Ln* (A/A_0) versus *t*.

3. Results and discussion

3.1. ZnS-AHA Nanoparticles characterization

The FTIR spectrometer was used to measure the vibrational frequencies of bonds in the molecules and to confirm the presence of different functional groups on the surface of ZnS nanoparticles (**Fig. S2**). The absorption band at 540 cm^{-1} was observed due to the Zn-S stretching vibrations [3]. The presence of Zn-S vibration clearly indicated that ZnS NPs was successfully formed. Absorption peak was observed at 3319 cm^{-1} which is due to the alcohol/phenol group (-OH) stretching vibration [4]. The strong broad peak at 3665 cm^{-1} is

attributed to N-H stretching mode of the secondary amides coming particularly from the identified molecule dihydroxanthin of plant extract [5]. The peak at 2978 cm^{-1} is probably ascribed to C-H alkane stretching, while the band at 2893 cm^{-1} could be assigned to the C–H stretching branched alkene, particularly from the identified molecule cis-hydroxydavanone compound of AHA extract [5]. The peak at 1575 cm^{-1} could be due to C=O carbonyl stretching group and the peak at 1057 cm^{-1} was assigned to the stretching vibrations of primary alcohol groups in the AHA extracts [6]. Hence, these two peaks confirmed the presence of flavonoids or polyphenolic compounds in AHA-capped ZnS NPs [6]. The peaks at 1393 and 1259 cm^{-1} corresponded to CH_3 and C-O stretching vibration coming mainly from the identified molecule vulgarin [5]. FTIR analysis evidenced that green nanoparticles were stabilized with the major phytoconstituents of AHA extract.

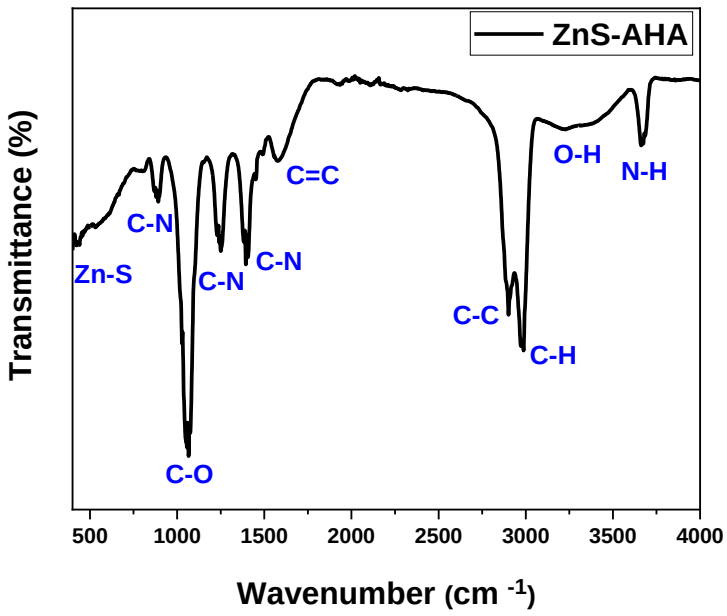

Fig. S2: FTIR spectrum of AHA-capped ZnS nanoparticles.

The crystal structures of the as-synthesized ZnS nanoparticles prepared using AHA as a capping agent was studied by X-ray diffraction (XRD) and the obtained XRD patterns are shown in **Fig. S3**. The diffraction peaks are broadly confirming the nanometric size of the ZnS particles. For the phase identification, diffraction patterns of the ZnS were compared and analyzed using the diffraction standards of the wurtzite phase (JCPDS card No.80-0020) and zinc blend phase (JCPDS card No.80-0007). XRD patterns can be indexed as cubic zinc blende structure, and they appear in good agreement with JCPDS data card No. 80-0007 with

prominent peaks corresponding to the reflections at (111) (220) and (311) planes. The non-appearance of diffraction peaks related to the wurtzite phase demonstrates that AHA capping favors the cubic structure. To better quantify the effect of the stabilizers, the size of the nanoparticles was estimated using the Scherrer formula [7]:

$$D = \frac{K\lambda}{\beta \cos(\theta)} \quad \text{(S.1)}$$

Where D is the average crystallite size (Å), k = 0.9 is the Scherrer constant, λ is the wavelength of X-ray (1.5402 Å) Cu Kα radiation, β is the full width at half maximum of the diffraction peak (in radian) and θ is the Bragg diffraction angle, respectively. The estimated average size of the ZnS-AHA nanocrystals was found to be nearly equal to 4 nm. The smaller size of the ZnS crystallites encapsulated by AHA extract is most likely due to the strong interaction of AHA molecules with ZnS nanocrystals which makes the growth slower [8]. On the other hand, the lattice constant of the cubic phase of ZnS nanocrystals can be estimated using the following expressions:

$$d_{hkl}^2 = \frac{a_c^2}{h^2+k^2+l^2} \quad \text{(S.2)}$$

Where d_{hkl} is the inter-reticular distance for the cubic structure; h, k, and l are Miller indices; λ is the wavelength of the X-ray radiation; a_c, *is* the lattice constant of the cubic phase of ZnS nanocrystals. The calculated average value of the lattice and the inter-reticular distance parameters of AHA ZnS nanocrystals was a= 5.4 Å and d_{hkl}=0.31 nm. It should be kept in mind that the Scherrer formula considers only the size effects coming from the diffraction results, and it then offers a lower limit for the nanocrystals size and neglects the micro-strain [9].

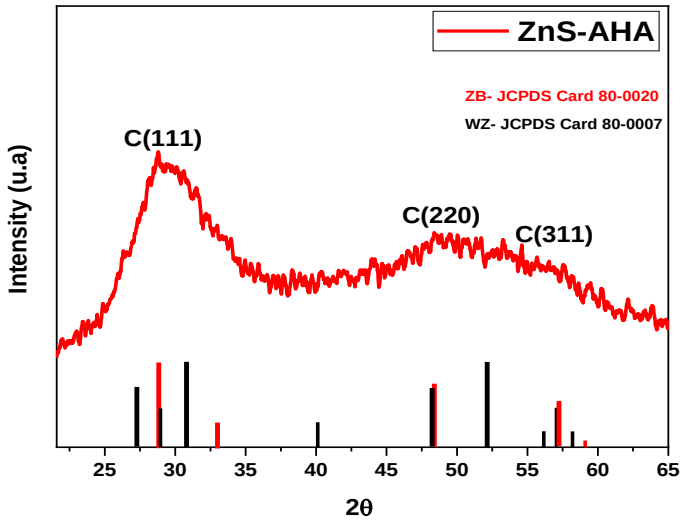

Fig. S3: DRX patterns of AHA-capped ZnS nanocrystals.

Figure S4a shows the HR-TEM images of the AHA-capped ZnS NPs, which are round, and a histogram of their sizes. Their aggregation could be due to the high concentration of nanoparticles. The histogram of nanocrystal size distribution shows that the average crystal size is 4.3 ± 0.5 nm. These results are in good agreement with the XRD results. The d-spacing determined from the digital micrograph for ZnS is 0.30 nm, which is close to the spacing of (111) diffraction plane of the cubic phase [2]. Comparing the values calculated by Bragg law, it is evident that the growth of ZnS-AHA occurs preferentially along the direction [111]. NPs elemental composition was determined by EDX (**Fig. S4b**). Zn and S are the major elemental components. The presence of C is related to the TEM grid and other peaks, Si and P, are probably due to residues coming from the synthesis and the grid.

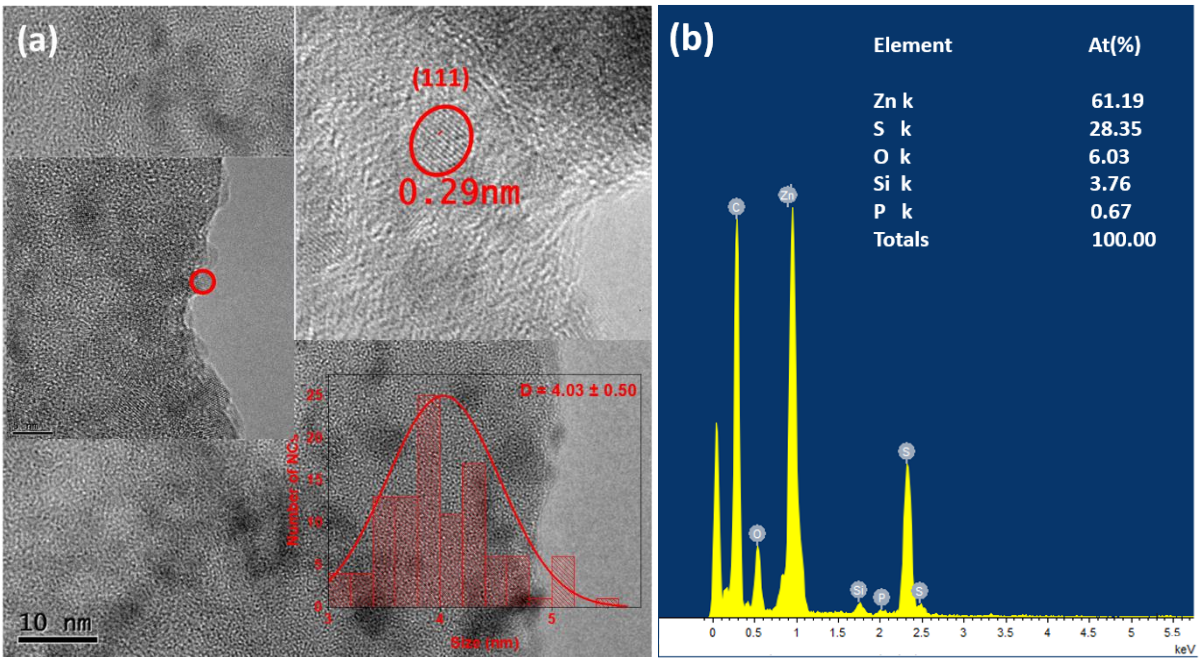

Fig. S4: (a) HR-TEM images of ZnS-AHA nanocrystals with an inset showing the 0.29 nm lattice spacing that corresponded to the (111) plane and (b) EDX results.

3.1.2. Optical study of ZnS-AHA NPs

In order to investigate the optical properties and the impact of ligand on the stability and size distribution of the nanoparticles, the optical absorption spectra of the ZnS NAs dispersed in water were recorded in (**Fig. S5**). The UV-Visible absorption spectrum of ZnS NAs suspension shows an absorption band at 325 nm related to the first electronic transition $1S_e$-$1S_h$ [10]. The blue shift compared to bulk ZnS (344 nm, E_g = 3.6 eV) is due to the quantum

confinement of charge carriers due to the small particle size. This tendency is characteristic of semiconductors II-VI, mainly associated with the nanocrystal size distribution and sub-bandgap transitions arising from the intrinsic-extrinsic defect states. We have determined

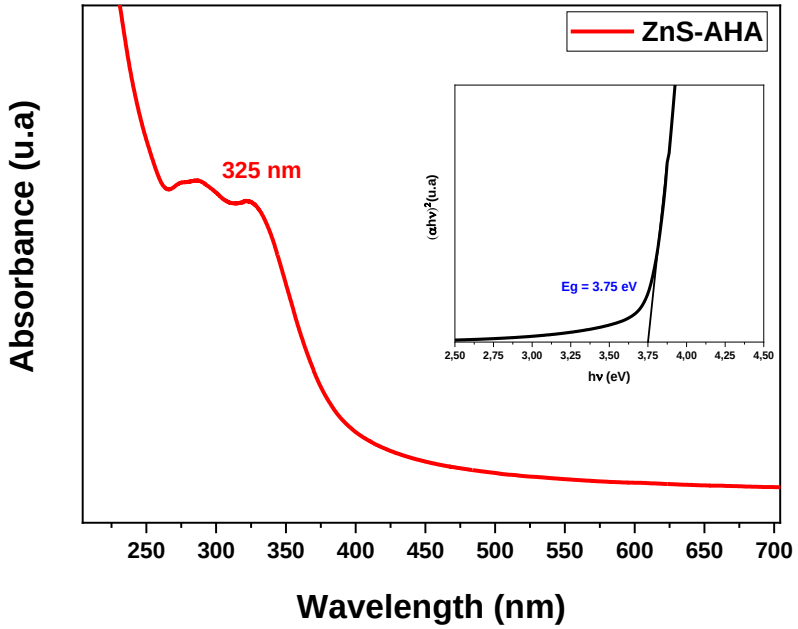

graphically the value of the optical and band-gap energy *Eg* using the following Tauc relation [11]:

$$\alpha h\nu = A\,(h\nu - Eg)^n \qquad \text{(S.3)}$$

Here, α is the absorption coefficient, A is a constant, h is the Planck constant, ν is the frequency of radiated photons and n is a transition-dependent factor (n = 1/2 for direct semiconductors). The optical gap energy of the capped ZnS NPs is obtained by extrapolating the plot of the function $(\alpha h\nu)^2$ to the value α = 0. The intersection of the line with the horizontal axis gives the band gap energy value, (see insert in **Fig. S5**). The estimated band gap energy for the green ZnS is 3.70 eV. It is clear that the gap energy of these ZnS NPs shifts towards the blue, compared to that of the bulk ZnS (E_g = 3.6 eV); this is due to the very small size of NPs, which induces a quantum confinement effect (QCE) [12].

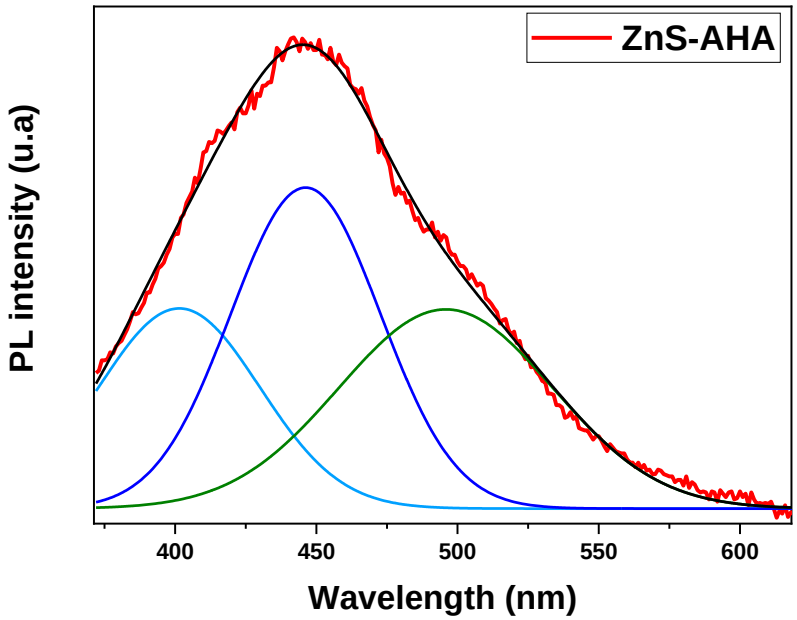

Fig. S5: Absorption spectra for ZnS nanoparticles prepared with AHA plant extract. The determination of the energy band gap using Tauc Relation is shown in the inset.

Fig. S6 shows the emission spectra of ZnS NPs obtained with an excitation wavelength λ_{exc}= 325 nm at room temperature. An intense and wide band centered at 450 nm dominates the spectrum. The emission spectra are deconvoluted using three Gaussian profiles associated with three main bands. The first band is less intense and has a spectral width of a few nm and is strongly correlated with the size of the nanoparticles. This band was attributed to the direct band-to-band recombination of excitons. The second emission band in the blue region (450 nm), which dominates the spectrum, was attributed to recombination between electrons and holes at the edges of conduction and valence bands respectively, or involves very shallow recombination centers (sulfur vacancies Vs) [13]. Finally, the green emission band (500 nm) was attributed to the interstitial zinc atom (I_{Zn}) [14]. The FWHM of the main emission band is equal to 62 nm which is related to the size dispersion of the ZnS-AHA NPs.

Fig. S6: Gaussian adjustment of PL spectra of AHA capped ZnS NPs.

References

[1] S. Ouni, N. Mohamed, M. Bouzidi, A. Bonilla-Petriciolet, M. Haouari, High impact of thiol capped ZnS nanocrystals on the degradation of single and binary aqueous solutions of industrial azo dyes under sunlight, J. Environ. Chem. Eng. 9 (2021) 105915. https://doi.org/10.1016/j.jece.2021.105915.

[2] N. Mohamed, S. Ouni, B. Mohamed, M. Bouzidi, A. Bonilla-Petriciolet, M. Haouari, Synthesis and preparation of acid capped CdSe nanocrystals as successful adsorbent and photocatalyst for the removal of dyes from water and its statistical physics analysis, Environ. Sci. Pollut. Res. (2022). https://doi.org/10.1007/s11356-022-20990-9.

[3] D. Amaranatha Reddy, C. Liu, R.P. Vijayalakshmi, B.K. Reddy (2014) Effect of Al doping on the structural, optical and photoluminescence properties of ZnS nanoparticles, J. Alloys Compd. 582: 257–264.

[4] H. Asoufi, T. Al-Antary, A. Awwad (2018) biosynthesis and characterization of iron sulfide (FeS) nanoparticles and evaluation their aphicidal activity on the green peach aphid myzus persicae (Homoptera: aphididae), Fresenius Environ. Bull. 27: 7767–7775.

[5] Q.F. Nafa, S.M. Hussin, W.F. Hamadi (2021) Characterization of some active organic compound from Cold and Hot aqueous solvent and Study their Antibiotic of Artemisia herba-alba Asso plant oil, Egypt. J. Chem. 64: 6691–6709.

[6] U.S. Senapati, D. Sarkar, Structural (2015) spectral and electrical properties of green synthesized ZnS nanoparticles using Elaeocarpus floribundus leaf extract, J. Mater. Sci. Mater. Electron. 26: 5783–5791.

[7] M. Adoni, M. Yadam, S. Gaddam, R. Usha, V.S. Kotakadi, Antimicrobial, Antioxidant, and Dye Degradation Properties of Biosynthesized Silver Nanoparticles From Artemisia Annua L, Lett. Appl. NanoBioScience. 10 (2021) 1981–1992. https://doi.org/10.33263/LIANBS101.19811992.

[8] Y. Yu, L. Xu, J. Chen, H. Gao, S. Wang, J. Fang, S. Xu (2012) Hydrothermal synthesis of GSH–TGA co-capped CdTe quantum dots and their application in labeling colorectal cancer cells, Colloids Surf. B Biointerfaces. 95: 247–253.

[9] M. Jothibas, C. Manoharan, S. Johnson Jeyakumar, P. Praveen, I. Kartharinal Punithavathy, J. Prince Richard (2018) Synthesis and enhanced photocatalytic property of Ni doped ZnS nanoparticles, Sol. Energy. 159: 434–443.

[10] V. Mote, Y. Purushotham, B. Dole (2012) Williamson-Hall analysis in estimation of lattice strain in nanometer-sized ZnO particles, J. Theor. Appl. Phys. 6: 6.

[11] H. Matsumoto, T. Sakata, H. Mori, H. Yoneyama (1996) Preparation of Monodisperse CdS Nanocrystals by Size Selective Photocorrosion, J. Phys. Chem. 100: 13781–13785.

[12] L. Meng, A. Maçarico, R. Martins (1995) Study of annealed indium tin oxide films prepared by rf reactive magnetron sputtering, vacuum. 46: 673–680.

[13] N. Ben Brahim, M. Poggi, N.B. Haj Mohamed, R. Ben Chaâbane, M. Haouari, M. Negrerie, H. Ben Ouada (2016) Synthesis, characterization and spectral temperature-dependence of thioglycerol-CdSe nanocrystals, J. Lumin. 177: 402–408.

[14] Y. Piña-Pérez, O. Aguilar-Martínez, P. Acevedo-Peña, C.E. Santolalla-Vargas, S. Oros-Ruíz, F. Galindo-Hernández, R. Gómez, F. Tzompantzi (2018) Novel ZnS-ZnO composite synthesized by the solvothermal method through the partial sulfidation of ZnO for H2 production without sacrificial agent, Appl. Catal. B Environ. 230: 125–134.